Perpendicular Domain Orientation in Thin Films of Polystyrene−Polylactide Diblock Copolymers

Roberto Olayo-Valles,[†] Shouwu Guo,[‡] M. S. Lund,[†] C. Leighton,[†] and Marc A. Hillmyer*,[‡]

Department of Chemical Engineering and Materials Science, University of Minnesota, Minneapolis, Minnesota 55455, and Department of Chemistry, University of Minnesota, Minneapolis, Minnesota 55455

Received April 27, 2005; Revised Manuscript Received September 17, 2005

ABSTRACT: Block copolymer thin films are ideal templates for a wide range of technologies where large area patterns of nanoscale features are desired. One of the main challenges in using lamellae- and cylinder-forming block copolymers for this purpose is to induce the block copolymer domains to orient perpendicular to the film surface. We here show that perpendicular domain orientation can be easily achieved with polystyrene-*b*-polylactide (PS−PLA) thin films. Cylinder-forming PS−PLA films were prepared by spin-coating on a variety of substrates followed by thermal annealing. The molecular weight, film thickness, annealing temperature, and annealing time were varied. When the film thickness was larger than the repeat spacing of the bulk morphology, the domains oriented perpendicular to the surface independent of the substrate/film interface. The films were then used to prepare nanoporous templates by a combination of hydrolytic PLA degradation and oxygen reactive ion etching (O_2-RIE). The template pattern was then transferred to the substrate using CF_4-RIE to form an array of nanoscale pits.

Introduction

The self-assembly properties and the ease of processing of block copolymers make them ideal materials for the development of novel technologies where large area patterns of nanoscale features are desirable.[1−4] In particular, cylinder-forming (*C*) block copolymer thin films have been used to prepare membranes[5] and nanoparticle deposits[6] and as templates for the fabrication of nanodot and nanowire arrays[7−12] as well as for pattern transfer to an underlying substrate.[13] Block copolymer thin films can be easily prepared by spin-coating on a number of substrates. The main challenge, however, in using *C* films for the applications listed above is to tailor the self-assembly process to spontaneously form cylinders with their long axis oriented perpendicular to the film surface ($C_\perp$).

The self-assembly process of block copolymers in thin film form is strongly influenced by the presence of the air/film surface and the film/substrate interface.[14] Generally, the components with the lowest surface and interface energies tend to form layers at the surface and substrate interface, respectively.[15−18] In thin films with lamellar morphology (*L*), the formation of these layers dominates the orientation of the domains and induces an ordering of the lamellae parallel to the substrate ($L_{||}$), provided the overall film thickness (t) is larger than the repeat spacing of the lamellae.[17,18] On the surface of these films, islands and holes form so that the local thickness is commensurate with an integer number of lamellae.[19,20] If the substrate is neutral in its interaction with both blocks, which can be achieved by anchoring a random copolymer brush to its surface or by employing self-assembled monolayers,[21,22] a hybrid structure is formed with lamellae oriented perpendicular to the substrate ($L_\perp$) near the interface and $L_{||}$ orientation near the surface.[23,24] Self-consistent-field theory (SCFT) confirms that $L_\perp$ orientation is more favorable at a neutral interface due to higher conformational freedom of the polymer molecules near the interface.[25] Recently, Xu et al. used cross-section TEM to show that the depth to which the surface affects the structure of a *L* film is determined by the difference in interfacial energies between each of the block copolymer components and the surface (ξ).[26]

In thin films of asymmetric block copolymers that form cylinders in the bulk state, the thermodynamic interactions at the interfaces and t not only affect the orientation of the cylinders, which may orient with their long axis parallel ($C_{||}$) or perpendicular ($C_\perp$) to the surface, but can also cause a change in the morphology near the interface (or the surface) to lamellae, spheres, or perforated lamellae.[27−32] Theoretical work on cylinder-forming films has been less extensive than their lamellar counterparts due in part to the difficulty of implementing the appropriate SCFT in three dimensions.[14,33,34]

Huinink et al. used dynamic density functional theory (DDFT) simulations of cylinder-forming diblock copolymers films constrained between two similar interfaces (i.e., a symmetrical constraint) and mapped the changes in morphology and orientation as a function of film thickness and ξ.[35,36] They predicted that when $\xi = 0$, the minority block preferentially wets the surface due to an entropic effect. An effectively neutral surface, therefore, will be one with slight energetic preference for the majority block, which then balances this entropic effect. When such a surface is employed in the simulations, $C_\perp$ is formed at all thicknesses. Similar results were obtained by Wang et al. using Monte Carlo simulations.[37] Knoll et al. experimentally observed the dependence of morphology and orientation on the thickness of films of an ABA cylinder-forming triblock copolymer upon solvent annealing.[31] Their experimental results were explained using DDFT simulations of symmetrically constrained films similar to those of

[†] Department of Chemical Engineering and Materials Science.
[‡] Department of Chemistry.
* Corresponding author. E-mail: hillmyer@chem.umn.edu.

10.1021/ma0509006 CCC: $30.25
Published on Web 11/05/2005

Huinink et al.[31] In their simulations, Horvat et al. explored a wider parameter space and found that a disordered layer is predicted when t is considerably smaller than the center-to-center distance between nearest-neighbor cylinders in the bulk (d^*_{C-C}).[38] They also found that the interfaces affect the morphology of the film to a depth of $d^*_{C-C}/\sqrt{3}$ while in the middle of the film $C_{\parallel}$ is preferentially formed. Recently, Lyakhova et al. have performed DDFT simulations of cylinder-forming films with independent ξ at each interface (i.e., an asymmetric constraint).[39] They found that hybrid structures are formed when the two ξ are different and that two different orientations, such as $C_{\parallel}$ and $C_{\perp}$, can coexist in a single layer. Asymmetric constraints more closely reflect the nature of films with a free surface although not completely since these films can form islands and holes.

Experimentally, large-area films with $C_{\perp}$ orientation have been prepared by controlled solvent evaporation,[40,41] blending of small molecules or nanoparticles with the block copolymer combined with solvent or thermal treatment,[10,42,43] applying an electric field,[11,44] employing a neutral substrate,[11,45] and thermal annealing.[12,46,47] The latter can be used when the components of the block copolymer have similar surface energies. This methodology is simple and has the advantage of producing $C_{\perp}$ films even when t is much larger than d^*_{C-C}.[46]

We previously reported that thin films of a cylinder-forming polystyrene-*b*-polylactide (PS−PLA) diblock copolymer on a variety of substrates attain $C_{\perp}$ conformation at the surface upon thermal annealing.[12] The PS−PLA films were then used to form nanoporous templates through the combination of RuO_4 staining and O_2 reactive ion etching (O_2-RIE). The use of these templates to prepare magnetic nanodot arrays was demonstrated. In this paper we report the preparation of PS−PLA thin films of different molecular weights and the characterization of the self-assembled structure as a function of film thickness and annealing temperature. We found that $C_{\perp}$ is preferentially formed when $t > d^*_{C-C}$ at all the molecular weights and on all the substrates we tested. We propose that $C_{\perp}$ is formed due to the similar surface energy of PS and PLA. The $C_{\perp}$ orientation is prevalent at high annealing temperatures and after long annealing times, showing that this morphological arrangement is stable. Also, high annealing temperature results in a more uniform self-assembled pattern. Finally, we demonstrate a new route to form nanoporous templates by a combination of chemical degradation of PLA and O_2-RIE. This methodology avoids the use of RuO_4 staining, allowing easy removal of the template mask by simple dissolution. An array of nanopits in a Si(100) substrate was prepared by transferring the pattern of the nanoporous template to the substrate using CF_4-RIE.

Experimental Section

The synthesis and characterization of PS−PLA have been previously described.[48−50] Table 1 shows the molecular characteristics of the PS−PLA materials used in this work. The number-average molecular weight (M_n) and the volume fraction of PLA (f_{PLA}) were determined from ^{1}H NMR spectroscopy performed on Varian 300 VXR and Varian Inova 500 spectrometers. All of these materials self-assemble to form well-defined morphologies. The bulk morphology and its dimensions (Table 1) were characterized by small-angle X-ray scattering (SAXS). SAXS experiments were performed on a home-built beamline at the University of Minnesota. A Rigaku RU-200BVH rotating anode source fitted with a 0.2 × 2 mm^2 microfocus cathode, and Franks mirror optics was used to produce Cu Kα X-rays with a wavelength of 1.542 Å. Two-dimensional scattering patterns were recorded on a Siemens multiwire detector and corrected for detector response before analysis.

Table 1. Molecular and Bulk Morphological Characteristics of PS−PLA Samples

sample	M_n (kg/mol)[a]	f_{PLA}[b]	d^*_{C-C} (nm)[c]	D (nm)[d]
SL-A	96.0	0.36	69	44
SL-B	60.5	0.29	49	27
SL-C	26.6	0.26	30	16
SL-lam	41.0	0.53	32[e]	

[a] Number-average molecular weight determined by ^{1}H NMR spectroscopy.[49] [b] PLA volume fraction determined from ^{1}H NMR spectroscopy and densities at 110 °C (ρ_{PS} = 1.02 g/cm^3, ρ_{PLA} = 1.18 g/cm^3). [c] Center-to-center distance between closest-neighbor PLA cylinders determined from small-angle X-ray scattering. [d] Diameter of PLA cylinders determined from d_{C-C} assuming hexagonal packing of PLA cylinders and constant density. [e] Lamellar spacing.

Thin films of PS−PLA were prepared on Si(100) with an amorphous native oxide layer, Al_2O_3(0001), MgO(100), and GaAs(001) single-crystal substrates, and on polycrystalline Al, Au, Cu, and SiO_2 seed layers. The seed layers were prepared by dc and rf magnetron sputtering on Si(100) substrates. Additionally, the surface of some Si(100) substrates was further modified. This was done by first sonicating the Si(100) wafer in dichloromethane, methanol, and deionized water for 10 min each followed by immersion in a 5:1:1 $H_2O/H_2O_2/NH_3$ solution for 1 h at 100 °C to generate hydroxide-functionalized hydrophilic surfaces. After fully rinsing in water and drying with compressed N_2 gas, the substrates were transferred to a 0.5% hexamethyldisilazane (HMDS, Electron Microscopy Sciences) solution in dry toluene and kept in the solution for 16 h to form hydrophobic surfaces. Finally, the substrates were rinsed with toluene and stored under vacuum for future use.

Solutions of PS−PLA in chlorobenzene (Aldrich) and toluene (Aldrich) were used to prepare thin films by spin-coating. In all cases the spinning speed was 2000 rpm, and the concentration of the solutions was varied to obtain films with different thicknesses. The films were annealed under vacuum (0.01 Torr) at different temperatures. Film thickness was measured by X-ray reflectivity or atomic force microscopy (AFM). X-ray reflectivity was performed on a Phillips X'Pert diffractometer equipped with a 1.8 kW ceramic copper X-ray tube source, a graded parabolic mirror with automatic attenuator, and $^1/_2$° divergence slit. The diffracted beam arm was equipped with a parallel plate collimator with a 0.1 mm collimator slit and a proportional counter. AFM was used to measure film thickness by first scratching the films in at least three different places with a razor blade followed by scanning across the scratch edges. AFM was performed in tapping mode on a Nanoscope IIIa multimode system (Veeco Instruments) using Olympus tapping mode etched silicon probes (Veeco Instruments) (force constant ∼ 42 N/m, resonance frequency 200−400 kHz). All data, height and phase, were acquired under ambient conditions using an engage set point of 0.9, free amplitude of about 50 nm, and scanning rates ranging from 0.75 to 1 Hz. Table 2 contains the thicknesses of the films prepared on Si(100) with native oxide. The standard deviation of thickness measurements performed by X-ray reflectivity was calculated from the measurements of at least three different films. In the case of AFM measurements, the standard deviation was calculated from the measurements on the different scratches on the same film.

The morphology of the films at the surface was imaged by scanning electron microscopy (SEM) and AFM. Scanning electron microscopy was performed on Hitachi S900 and JEOL 6700 microscopes, both equipped with field-emission gun sources, in secondary electron imaging mode, at an accelerating voltage of 1.0 keV. Natural contrast between PS and PLA

Table 2. Thickness of Films Prepared from Chlorobenzene Solutions and Supported on Si(100) with Native Oxide

	thickness (nm)	
concn (mg/mL)[a]	SL-A	SL-B
5	24 ± 1 [b]	14 ± 2 [b]
10	51 ± 4 [b]	44 ± 4 [c]
15	73 ± 5 [b] (75 ± 2 [c])	75 ± 3 [c]
20	111 ± 1 [c]	101 ± 4 [c]
30	158 ± 6 [c]	150 ± 2 [c]
40	324 ± 2 [c]	257 ± 14 [c]

[a] Concentration of solution from which film was prepared. [b] Measurements ±1 SD done by X-ray reflectivity. [c] Measurements ±1 SD done by AFM.

domains was observed. In some cases, however, films were treated with vapors of a 0.5% RuO_4 aqueous solution (Polysciences) to increase the contrast in SEM imaging and reduce charging effects. RuO_4 vapors selectively react with PS. The incorporation of Ru atoms to the PS domains increases the secondary electron yield from these domains which therefore appear brighter in the SEM image. Comparison between images of stained and nonstained films allowed us to identify the PS domains as the bright and PLA as dark regions in images of nonstained films. At least four SEM images were obtained for each sample, and they were analyzed to determine feature size and spacing between features. PS−PLA films were also imaged by AFM in tapping mode. The difference in viscoelastic properties between the softer PLA domains and the harder PS domains allowed us to image the morphology using phase imaging mode.

Nanoporous films were prepared by immersing the PS−PLA films in 0.5 or 0.05 M solutions of NaOH (Aldrich) in methanol/water (40 vol % methanol) at room temperature to degrade and remove a portion of the PLA. The films were further etched by O_2-RIE (70 mTorr, 60 W) for 10 s to ensure that the pores extend through the entire film. The pattern of the nanoporous film was transferred to the Si(100) substrate by exposing it to CF_4-RIE (30 mTorr, 120 W) for 10 s, forming nanopits on the substrate. The polymer film was then removed by dissolution in chlorobenzene.

Results and Discussion

Thin films of PS−PLA samples SL-A and SL-B, whose characteristics are presented in Table 1, were prepared on Si(100) with a native oxide layer (ca. 100 nm thick) by spin-coating from solutions of variable concentration to obtain films with different thicknesses. The thicknesses of the films are shown in Table 2. Two methods were employed to measure the thickness of the films: X-ray reflectivity and AFM. A comparison between the two methods was made on films of SL-A prepared from solutions with concentration of 15 mg/mL. The difference between the two measurements was within experimental error as can be seen in Table 2. Thin film samples are designated as SL-*X*-*Y*, where SL-*X* is the PS−PLA sample used (Table 1) and *Y* is the thickness of the film in nanometers. Figure 1 shows SEM images of SL-A films after spin-coating. We have previously determined that the light regions of the image correspond to PS and dark to PLA by comparing images between films stained with RuO_4 and unstained films.[12] On the surface of SL-A-24 we observed predominantly $C_{||}$. As the thickness of the films was increased, mixed $C_{||}$ and $C_{\perp}$ were observed, except in film SL-A-158 where we observed predominantly $C_{||}$.

After the films of SL-A were annealed under vacuum for 12 h at 110 °C, above the glass transition temperatures of both PS and PLA, islands were formed on SL-A-24 (Figure 2). On SL-A-51 films, islands and holes

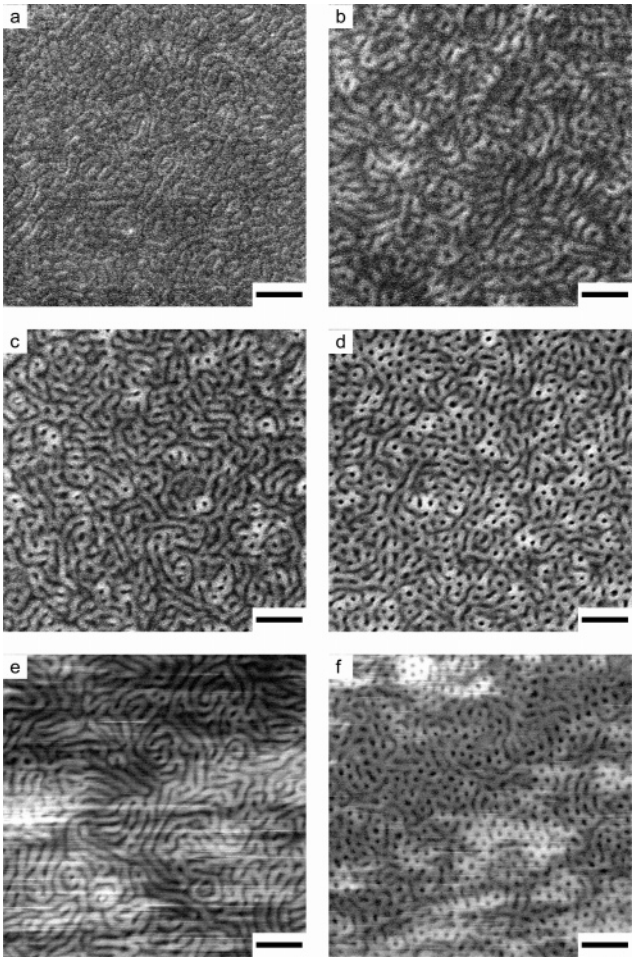

Figure 1. SEM images of films of (a) SL-A-24, (b) SL-A-51, (c) SL-A-73, (d) SL-A-111, (e) SL-A-158, and (f) SL-A-324 supported on Si(100) with native oxide layer after spin-coating. Scale bar 250 nm.

were observed. In both SL-A-24 and SL-A-51, hexagonally packed circular features were observed on the surface of the islands. On thicker films (73−324 nm) smooth surfaces with predominantly $C_{\perp}$ were observed. The roughness of an annealed SL-A-73 film was measured by AFM to be 2 nm over an area of 100 μm^2.

SL-A-73 films were also annealed at 130, 170, 210, and 240 °C for 12 h.[51] As can be seen in the SEM images shown in Figure 3, the $C_{\perp}$ orientation is prevalent in all cases and as the annealing temperature is increased, the PLA domains have a more regular shape. For each annealing temperature, at least four images at the magnification shown in Figure 3 were analyzed to determine d^*_{C-C} as well as size (D) and eccentricity of the PLA domains.[52] The average values are plotted in Figure 4. At all four temperatures D remains constant around 38 nm, slightly lower than the bulk value of 44 nm. As the annealing temperature was increased, the eccentricity of the domains decreased and d^*_{C-C} increased. We attribute the decrease in eccentricity to the higher mobility of the polymer molecules at elevated temperatures.[53] ^{1}H NMR spectroscopy of the films after annealing above 210 °C showed that the PLA was thermally degraded during annealing.[54] Furthermore, holes were observed in SEM images of films annealed at 240 °C, as shown in Figure 5. We believe that during annealing above 210 °C some PLA chains degrade resulting in the formation of PS homopolymer which incorporates into the PS matrix and swells it. This

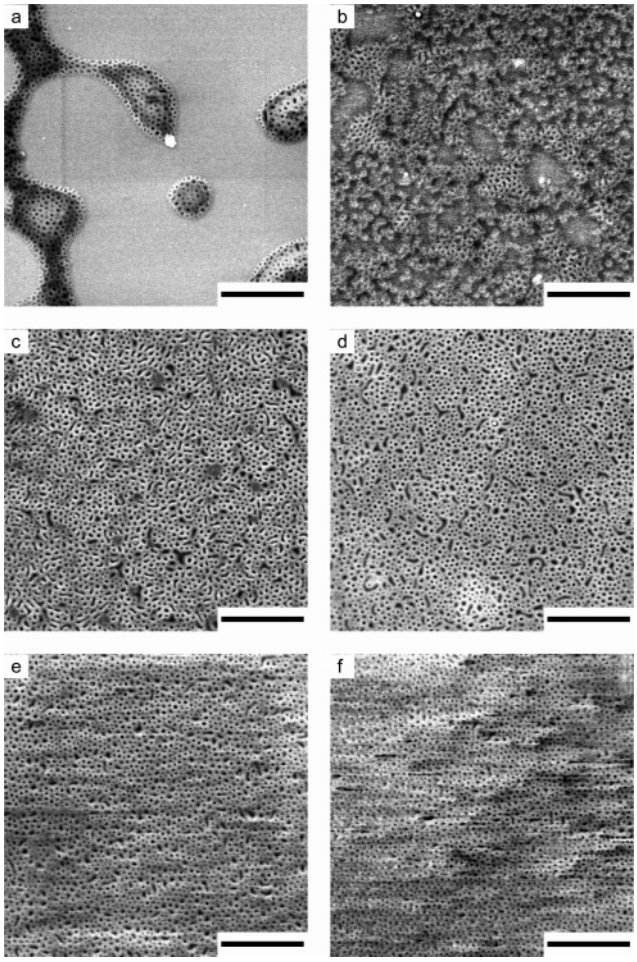

Figure 2. SEM images of films of (a) SL-A-24, (b) SL-A-51, (c) SL-A-73, (d) SL-A-111, (e) SL-A-158, and (f) SL-A-324 supported on Si(100) with native oxide layer after thermal annealing at 110 °C for 12 h. Scale bar 1 μm.

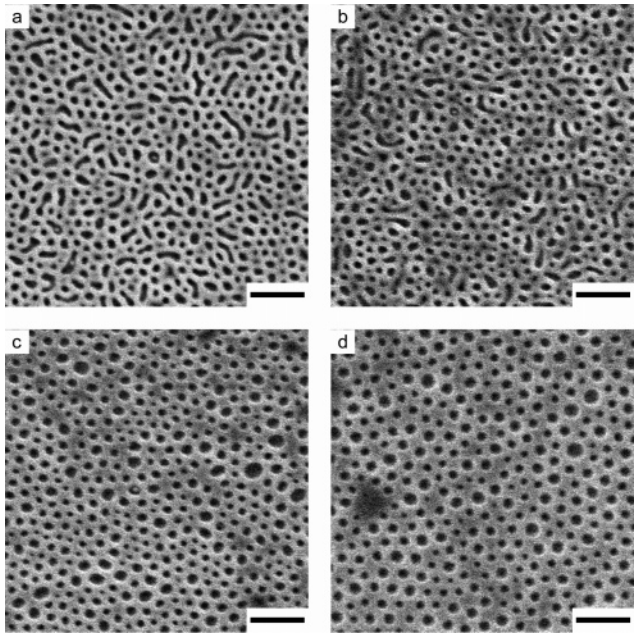

Figure 3. SEM images of SL-A-73 films supported on Si(100) with native oxide layer annealed for 12 h at (a) 130, (b) 170, (c) 210, and (d) 240 °C. Scale bar 100 nm.

causes the increase in d^*_{C-C}. We also annealed SL-A-73 films at 130 °C for up to 57 h. An increase in d^*_{C-C} was

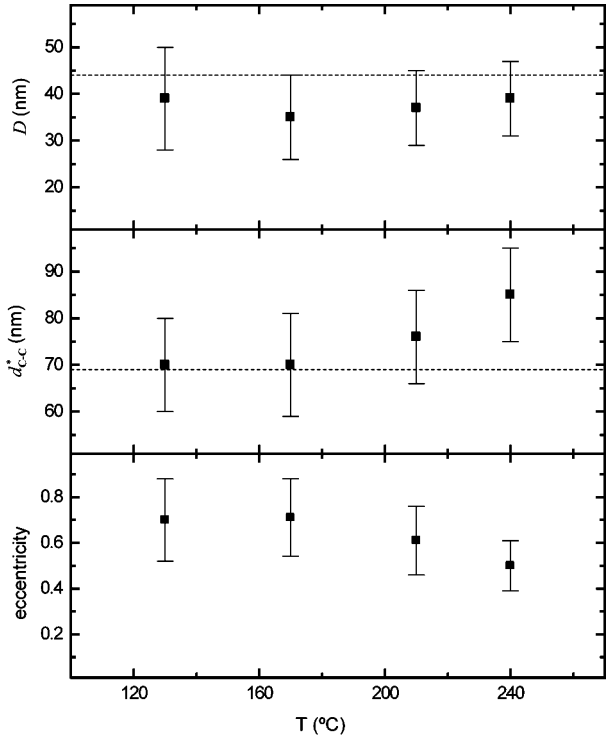

Figure 4. Plots of average D, d^*_{C-C}, and eccentricity (±1 standard deviation) of PLA domains of SL-A-73 films supported on Si(100) with native oxide layer as a function of annealing temperature.

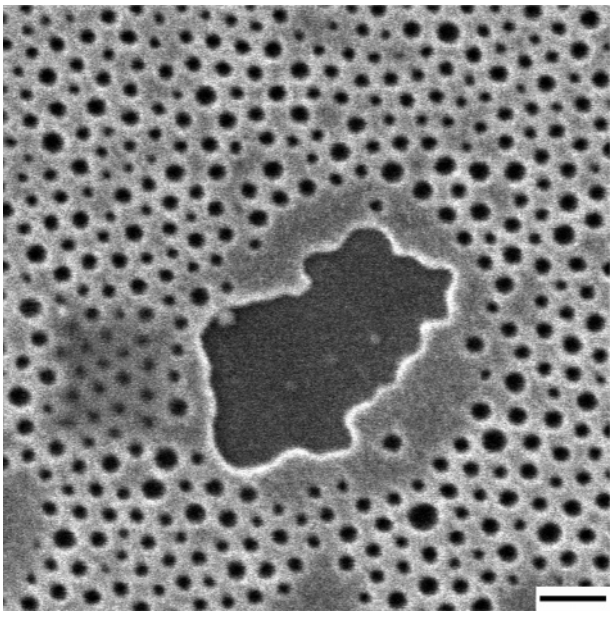

Figure 5. SEM image of SL-A-73 film supported on Si(100) with native oxide layer annealed at 240 °C for 12 h. The film was stained with RuO_4 vapors. Scale bar 200 nm.

also observed for the longer annealing times which we believe is also caused by the partial thermal degradation of PLA.

Thin films of SL-B were prepared in the same manner. For thinner films, SL-B-14 and SL-B-44, we observed mixed $C_{\parallel}$ and $C_{\perp}$. With increasing film thickness, $C_{\perp}$ becomes more prevalent, and on the surface of SL-B-150 and SL-B-257 we only observed $C_{\perp}$. After annealing the SL-B films at 110 °C (Figure 6), we observed no or few features on the surface of the SL-B-14 films. All other SL-B films show predominantly $C_{\perp}$ orientation

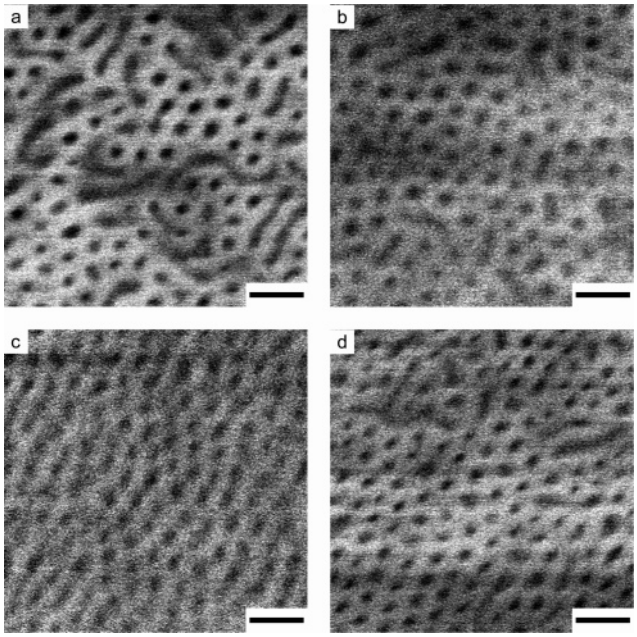

Figure 6. SEM images of films of (a) SL-B-75, (b) SL-B-101, (c) SL-B-150, and (d) SL-B-257 supported on Si(100) with native oxide layer after thermal annealing at 110 °C. Scale bar 100 nm.

after annealing, although some elongated features were also observed (e.g., Figure 6a).

These results show that the preferred self-assembled structure formed by SL-A and SL-B thin films at the surface is $C_\perp$ provided $t > d^*_{C-C}$. When $t < d^*_{C-C}$ upon annealing, we observe the formation of islands and holes or a featureless film. The surface energy of PLA depends on the conformation of the chains. Ringard-Lefebvre and Baszkin have measured the surface energy of PLA films prepared from acetone and chloroform solutions and report a range between 36 and 41.1 mJ/m^2.[55] This is very similar to the surface energy of PS which is reported to be 39.4−40.7 mJ/m^2.[56] Because of the similar surface energies, a neutrality condition exists at the air/film surface. This condition is responsible for the formation of $C_\perp$ at the surface.

Further proof that a neutrality condition exists at the surface was obtained from a thin film of PS−PLA with lamellar morphology (SL-lam, Table 1). A 70 nm thick film was prepared from a 15 mg/mL chlorobenzene solution. The thickness of the film was more than twice the lamellar repeat spacing (d_L = 32 nm). Figure 7 is an SEM image of the SL-lam film after annealing at 150 °C for 12 h. The fingerprint-like pattern is consistent with $L_\perp$ orientation. Theoretical and experimental studies have shown that if $t > d_L$ then $L_\perp$ is formed only when there is negligible difference in the components interfacial or surface energies.[14]

We also studied the effect of the substrate on the orientation of the cylinder-forming films. Films of SL-A from solutions with concentrations of 15 mg/mL were prepared on Al_2O_3(0001), GaAs(001), and MgO(100) single-crystal substrates as well as polycrystalline Al, Au, Cu, $Ni_{50}Mn_{50}$, and SiO_2 seed layers. Since the polymer, solution concentration and spin speed were similar to those used to prepare SL-A-73 films, the thickness of all the films was estimated to be about 73 nm.[57] After annealing at 210 °C for 12 h, films with predominantly $C_\perp$ were observed in all cases (Figure 8). Additionally, two other types of substrates were prepared by chemically modifying the surface of Si(100) with native oxide. Hydrophilic substrates were prepared by treating Si(100) wafers with hydrogen peroxide to introduce hydroxyl functionalities at the surface. Hydrophobic substrates were prepared by treating the hydroxyl-functionalized substrates with hexamethyldisilazane (HDMS). Films of SL-C were prepared on both hydrophilic and hydrophobic substrates from chlorobenzene solutions with concentrations of 15 mg/mL, resulting in a thickness of 60 nm. Figure 9 shows AFM images of an SL-C film on the hydrophobic substrate before and after annealing at 210 °C for 15 h. Again, $C_\perp$ was observed on the surface after annealing. The result was similar for the film supported on the hydro-

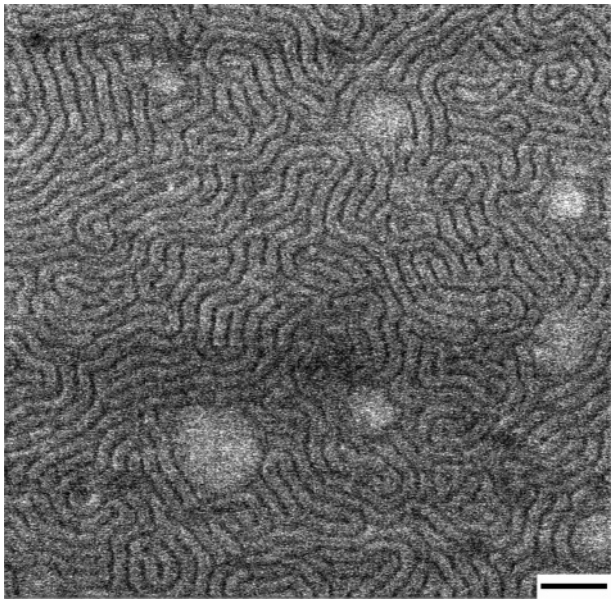

Figure 7. SEM image of a thin film of SL-lam supported on Si(100) with native oxide layer after annealing at 150 °C for 12 h. Scale bar 200 nm.

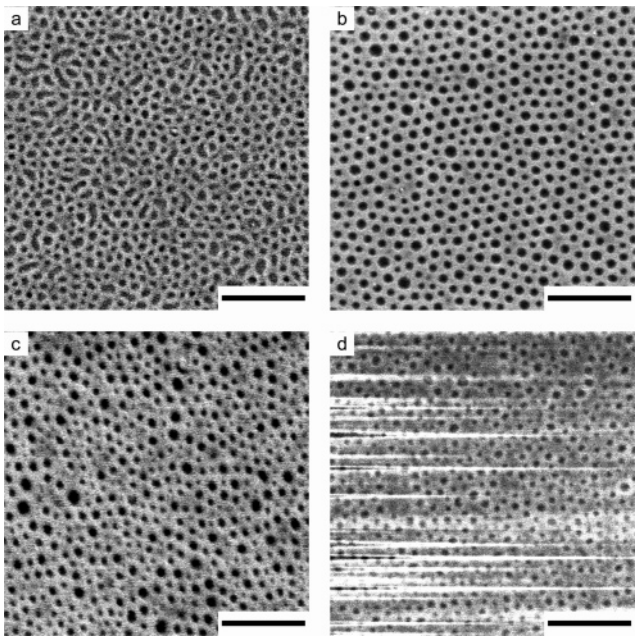

Figure 8. SEM images of films supported on (a) Al_2O_3(0001), (b) Al, (c) Cu, and (d) MgO after annealing at 210 °C for 12 h. The bright horizontal lines in image d are due to charging effects. Scale bar 500 nm.

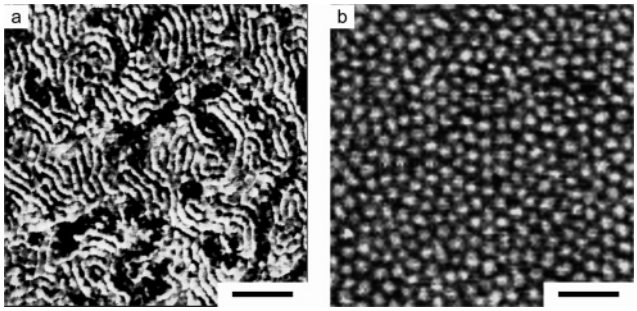

Figure 9. Topping mode AFM images of SL-C on a HDMS-modified Si(100) substrate before (a) and after (b) annealing at 210 °C for 15 h. Scale bar 200 nm.

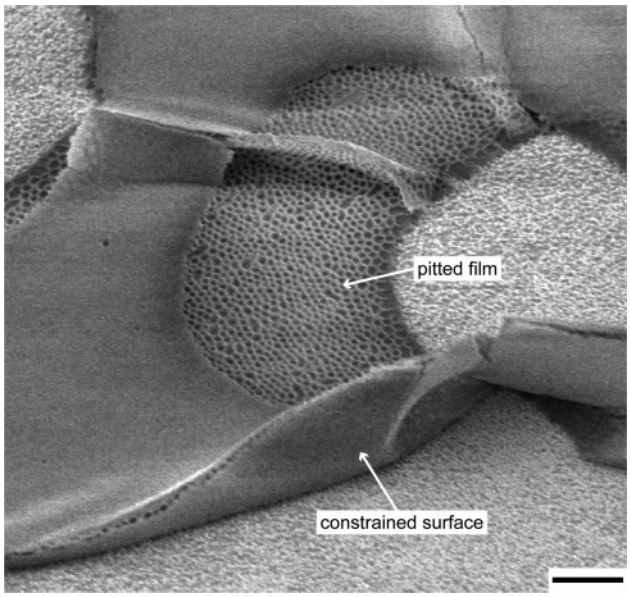

Figure 10. SEM image of SL-A-73 film on Si(100) with native oxide layer previously annealed at 170 °C and immersed in 0.5 M NaOH solution in methanol/water for 1.75 h. Scale bar 1 μm.

philic substrate. These results are further confirmation of the neutrality condition at the air/film surface.

To form porous films to be used as templates, we immersed previously annealed (170 °C 12 h) SL-A-73 films supported on Si(100) with native oxide layer in 0.5 M sodium hydroxide solution in methanol/water. After 2 h in the alkaline solution, 93% of the PLA was degraded as determined by ^{1}H NMR spectroscopy. In the process, however, the film delaminated from the substrate. Although this prevented the use of these films as templates, it allowed us to observe the constrained surface of the film originally in contact with the substrate. Figure 10 shows an SEM image of one of these films after 1.75 h in the alkaline solution. As can be seen, the bottom surface is featureless, indicating that one of the components forms a continuous layer at the film−substrate interface. Since most of the PLA has been degraded, the continuous layer observed in the image is likely PS. This indicates that one of the components has preferential energetic interaction with the Si(100) substrate. This preferential interaction leads the formation of a wetting layer (W) at the film−substrate interface. We also expect PLA to more strongly interact with polar surfaces such as the native oxide layer on untreated Si(100) and thus the structure to be like that depicted in Figure 11a.

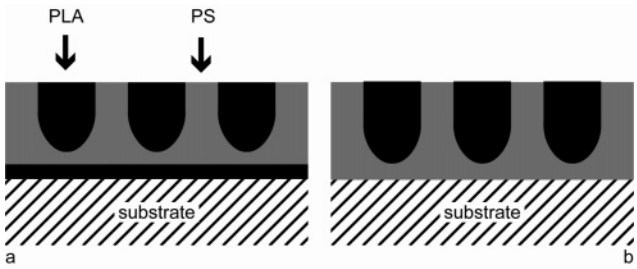

Figure 11. Cartoons showing the cross-section structure of the films when (a) PLA and (b) PS has the lowest interfacial energy.

The transverse structure of films supported on Si(100) consists then of $C_\perp$ at the surface and W near the substrate. For films with $t \simeq d^*_{C-C}$ such as SL-A-73 and SL-B-44 we expect a simple $W-C_\perp$ structure as shown in Figure 11.[39] When $t < d^*_{C-C}$, the formation of islands and holes is energetically favorable with $C_\perp$ formed on the surface of the islands and a featureless surface in the holes, which indicates the formation of a half lamellae or a disordered wetting layer. In the case of $t > d^*_{C-C}$ we have shown that $C_\perp$ is formed at the free surface, and we expect that W is formed near the substrate while theory predicts that $C_\parallel$ is formed between these layers.[39] However, this has not been experimentally confirmed.

SL-A-73 films on other substrates also delaminated after immersion in 0.5 M NaOH solution, except for films supported on HDMS-treated Si(100) which were significantly more stable. HDMS-treated Si(100) has a hydrophobic surface and thus we expect that the PS will have the lowest interfacial energy. We expect the structure of the film to be similar to that of Figure 11b. The HDMS−PS interface is stable in the alkaline solution and allowed us to immerse the films to degrade the PLA for at least 45 min without delamination. The greater stability of these films may be due to the absence of a degradable PLA layer or to better adhesion between PS and HDMS-treated Si(100) or both.

These findings allowed us to prepare nanoporous templates by a two-step process. First, we partially degraded the PLA to obtain nanopitted films. The pores on these films did not reach the substrate (Figure 11b). We then used O_2-RIE to complete the path of the pores to the substrate. We prepared templates from 60 nm thick films of SL-C supported on HDMS-treated Si(100). The films were immersed in alkaline solution, but the concentration of the solution was reduced to 0.05 M. Immersion of the films for 45 min resulted in degradation of ca. 77% of the PLA as measured by ^{1}H NMR spectroscopy. Longer immersion times resulted in partial delamination of the films. A tapping mode AFM height image of the film after the partial degradation of PLA is shown in Figure 12a. The film was then etched by O_2-RIE for 10 s so that the pores reach the substrate (Figure 12b). The template thus formed was used to produce nanopits on the substrate by exposing the sample to CF_4-RIE for 15 s followed by removal of the polymer film by simple dissolution in chlorobenzene (Figure 12c). If the O_2-RIE step is omitted, the nanopit array is not formed as can be seen in Figure 12d.

Conclusions

We have shown that PS−PLA thin films form perpendicularly oriented cylinders and lamellae due to the

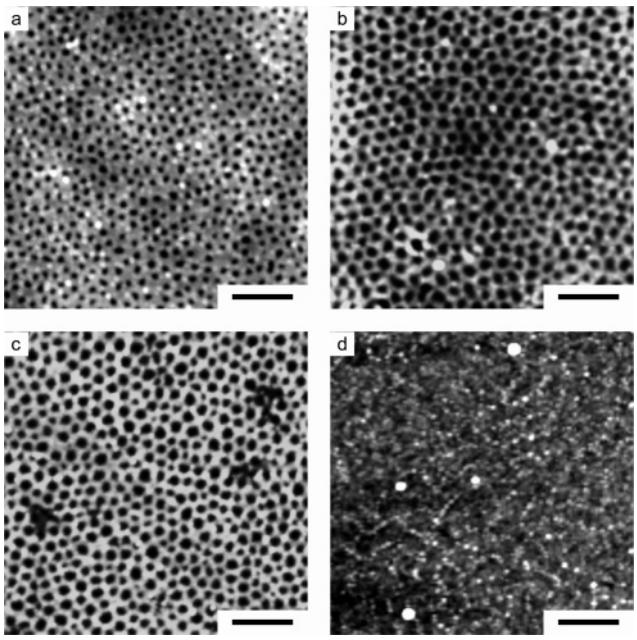

Figure 12. Tapping mode AFM topography (height) images of a SL-C film supported on HDMS-treated silicon after immersion in 0.05 NaOH in methanol/water for 30 min (a). The film was then etched by O_2-RIE for 10 s (b), followed by CF_4-RIE and dissolution of the template to form an array of nanopits (c). If the O_2-RIE step is omitted, the nanopits are not formed as shown in (d). Scale bar 200 nm.

similar surface energies of PS and PLA. In the case of films with cylindrical morphology, the $C_\perp$ orientation is formed independent of molecular weight and film thickness. Since a neutrality condition exists at the air/film surface, we were also able to prepare films with $C_\perp$ orientation on a variety of substrates. After annealing at temperatures as high as 240 °C and for long times, the $C_\perp$ orientation persisted which indicates that the observed structures are stable. Higher annealing temperatures produce more uniform patterns. However, annealing temperature and time have to be limited due to the thermal degradation of PLA. We utilized this structure to prepare a porous template using a two-step methodology: first we partially degraded the PLA by immersing the film in a NaOH solution; this was followed by a brief exposure to O_2-RIE to ensure the pores reach the substrate. The main advantage of this methodology is that the polymer template is not cross-linked and can thus be removed by simple dissolution. We demonstrated the applicability of these templates by transferring the template pattern to the Si(100) substrate by employing CF_4-RIE. Structures with higher aspect ratios may be possible using thicker films. To do this, the cross-section structure of the films and its changes with annealing will need to be studied.

Acknowledgment. This work was supported in part by the MRSEC program of the National Science Foundation under Award DMR-0212302, the National Science Foundation (DMR-0094144), the Industrial Partnership of Research in Interfacial and Materials Engineering (IPRIME) at the University of Minnesota, and the David and Lucile Packard Foundation. M.A.H. thanks Ullrich Steiner and Thomas Russell for helpful discussions and input.

References and Notes

(1) Hamley, I. W. *Nanotechnology* **2003**, *14*, R39−R54.
(2) Park, C.; Yoon, J.; Thomas, E. L. *Polymer* **2003**, *44*, 6725−6760.
(3) Lazzari, M.; López-Quintela, M. A. *Adv. Mater.* **2003**, *15*, 1583−1594.
(4) Hillmyer, M. A. *Adv. Polym. Sci.* **2006**, *189*, 137−181.
(5) Liu, G.; Ding, J. *Adv. Mater.* **1998**, *10*, 69−71.
(6) Misner, M. J.; Skaff, H.; Emrick, T.; Russell, T. P. *Adv. Mater.* **2003**, *15*, 221−224.
(7) Li, R. R.; Dapkus, P. D.; Thompson, M. E.; Jeong, W. G.; Harrison, C.; Chaikin, P. M.; Register, R. A.; Adamson, D. H. *Appl. Phys. Lett.* **2000**, *76*, 1689−1691.
(8) Thurn-Albrecht, T.; Schotter, J.; Kästle, G. A.; Emley, N.; Shibauchi, T.; Krusin-Elbaum, L.; Guarini, K.; Black, C. T.; Tuominen, M. T.; Russell, T. P. *Science* **2000**, *290*, 2126−2129.
(9) Shin, K.; Leach, K. A.; Goldbach, J. T.; Kim, D. H.; Jho, J. Y.; Tuominen, M.; Hawker, C. J.; Russell, T. P. *Nano Lett.* **2002**, *2*, 933−936.
(10) Sidorenko, A.; Tokarev, I.; Minko, S.; Stamm, M. *J. Am. Chem. Soc.* **2003**, *125*, 12211−12216.
(11) Thurn-Albrecht, T.; Steiner, R.; DeRouchey, J.; Stafford, C. M.; Huang, E.; Bal, M.; Tuominen, M.; Hawker, C. J.; Russell, T. P. *Adv. Mater.* **2000**, *12*, 787−791.
(12) Olayo-Valles, R.; Lund, M. S.; Leighton, C.; Hillmyer, M. A. *J. Mater. Chem.* **2004**, *14*, 2729−2731.
(13) Park, M.; Chaikin, P. M.; Register, R. A.; Adamson, D. H. *Appl. Phys. Lett.* **2001**, *79*, 257−259.
(14) Fasolka, M. J.; Mayes, A. M. *Annu. Rev. Mater. Res.* **2001**, *31*, 323−355.
(15) Thomas, H. R.; O'Malley, J. *Macromolecules* **1979**, *12*, 323−329.
(16) Hasegawa, H.; Hashimoto, T. *Macromolecules* **1985**, *18*, 589−590.
(17) Anastasiadis, S. H.; Russell, T. P.; Satija, S. K.; Majkrzak, C. F. *Phys. Rev. Lett.* **1989**, *62*, 1852−1855.
(18) Coulon, G.; Russell, T. P.; Deline, V. R.; Green, P. F. *Macromolecules* **1989**, *22*, 2581−2589.
(19) Coulon, G.; Collin, B.; Auserré, D.; Russell, T. P. *J. Phys. (Paris)* **1990**, *51*, 2801−2811.
(20) Collin, B.; Chatenay, D.; Coulon, G.; Auserré, D.; Gallot, Y. *Macromolecules* **1992**, *25*, 1621−1622.
(21) Mansky, P.; Liu, Y.; Huang, E.; Russell, T. P.; Hawker, C. J. *Science* **1997**, *275*, 1458−1460.
(22) Peters, R. D.; Yang, X. M.; Kim, T. K.; Sohn, B. H.; Nealey, P. F. *Langmuir* **2000**, *16*, 4625−4631.
(23) Huang, E.; Mansky, P.; Russell, T. P.; Harrison, C.; Chaikin, P.; Register, R. A.; Hawker, C. J.; Mays, J. *Macromolecules* **2000**, *33*, 80−88.
(24) Sohn, B. H.; Yun, S. H. *Polymer* **2002**, *43*, 2507−2512.
(25) Pickett, G. T.; Balazs, A. C. *Macromolecules* **1997**, *30*, 3097−3103.
(26) Xu, T.; Hawker, C. J.; Russell, T. P. *Macromolecules* **2005**, *38*, 2802−2805.
(27) Henkee, C. S.; Thomas, E. L.; Fetters, L. J. *J. Mater. Sci.* **1988**, *23*, 1685−1694.
(28) Liu, Y.; Zhao, W.; Zheng, X.; King, A.; Singh, A.; Rafailovich, M. H.; Sokolov, J.; Dai, K. H.; Kramer, E. J.; Schwarz, S. A.; Gebizlioglu, O.; Sinha, S. K. *Macromolecules* **1994**, *27*, 4000−4010.
(29) Radzilowski, L. H.; Carvalho, B. L.; Thomas, E. L. *J. Polym. Sci., Part B: Polym. Phys.* **1996**, *34*, 3081−3093.
(30) van Dijk, M. A.; van den Berg, R. *Macromolecules* **1995**, *28*, 6773−6778.
(31) Knoll, A.; Horvat, A.; Lyakhova, K. S.; Krausch, G.; Sevink, G. J. A.; Zvelindovsky, A. V.; Magerle, R. *Phys. Rev. Lett.* **2002**, *89*, 035501.
(32) Knoll, A.; Magerle, R.; Krausch, G. *J. Chem. Phys.* **2004**, *120*, 1105−1116.
(33) Suh, K. Y.; Kim, Y. S.; Lee, H. H. *J. Chem. Phys.* **1998**, *108*, 1253−1256.
(34) Turner, M. S.; Rubinstein, M.; Marques, C. M. *Macromolecules* **1994**, *27*, 4986−4992.
(35) Huinink, H. P.; Brokken-Zijp, J. C. M.; van Dijk, M. A.; Sevink, G. J. A. *J. Chem. Phys.* **2000**, *112*, 2452−2462.
(36) Huinink, H. P.; van Dijk, M. A.; Brokken-Zijp, J. C. M.; Sevink, G. J. A. *Macromolecules* **2001**, *34*, 5325−5330.
(37) Wang, G.; Nealey, P. F.; de Pablo, J. J. *Macromolecules* **2001**, *34*, 3458−3470.
(38) Horvat, A.; Lyakhova, K. S.; Sevink, G. J. A.; Zvelindovsky, A. V.; Magerle, R. *J. Chem. Phys.* **2004**, *120*, 1117−1126.
(39) Lyakhova, K. S.; Sevink, G. J. A.; Zvelindovsky, A. V.; Horvat, A.; Magerle, R. *J. Chem. Phys.* **2004**, *120*, 1127−1137.

(40) Kim, S. H.; Misner, M. J.; Xu, T.; Kimura, M.; Russell, T. P. *Adv. Mater.* **2004**, *16*, 226−231.
(41) Temple, K.; Kulbaba, K.; Power-Billard, K. N.; Manners, I.; Leach, K. A.; Xu, T.; Russell, T. P.; Hawker, C. J. *Adv. Mater.* **2003**, *15*, 297−300.
(42) Tokarev, I.; Krenek, R.; Burkov, Y.; Schmeisser, D.; Sidorenko, A.; Minko, S.; Stamm, M. *Macromolecules* **2005**, *38*, 507−516.
(43) Lin, Y.; Böker, A.; He, J.; Sill, K.; Xiang, H.; Abetz, C.; Li, X.; Wang, J.; Emrick, T.; Long, S.; Wang, Q.; Balazs, A.; Russell, T. P. *Nature (London)* **2005**, *434*, 55−59.
(44) Thurn-Albrecht, T.; DeRouchey, J.; Russell, T. P.; Kolb, R. *Macromolecules* **2002**, *35*, 8106−8110.
(45) Ryu, D. Y.; Shin, K.; Drockenmuller, E.; Hawker, C. J.; Russell, T. P. *Science* **2005**, *308*, 236−238.
(46) Ruokolainen, J.; Fredrickson, G. H.; Kramer, E. J.; Ryu, C. Y.; Hahn, S. F.; Magonov, S. N. *Macromolecules* **2002**, *35*, 9391−9402.
(47) Hammond, M. R.; Sides, S. W.; Fredrickson, G. H.; Kramer, E. J.; Ruokolainen, J.; Hahn, S. F. *Macromolecules* **2003**, *36*, 8712−8716.
(48) Zalusky, A. S.; Olayo-Valles, R.; Taylor, C. J.; Hillmyer, M. A. *J. Am. Chem. Soc.* **2001**, *123*, 1519−1520.
(49) Zalusky, A. S.; Olayo-Valles, R.; Wolf, J. H.; Hillmyer, M. A. *J. Am. Chem. Soc.* **2002**, *124*, 12761−12773.
(50) Mao, H.; Arrechea, P. L.; Bailey, T. S.; Johnson, B. J. S.; Hillmyer, M. A. *Faraday Discuss.* **2005**, *128*, 149−162.
(51) In ref 48 we reported that SL-A retains the cylinder morphology up to 270 °C.
(52) Eccentricity (e) is defined as $e = \sqrt{1 - b^2/a^2}$ where a is the semimajor axis and b is the semiminor axis of each ellipse fit to the dark round (elliptical) features (i.e., PLA domains) shown in Figure 3.
(53) Guarini, K. W.; Black, C. T.; Yeung, S. H. I. *Adv. Mater.* **2002**, *14*, 1290−1294.
(54) Jamshidi, K.; Hyon, S.-H.; Ikada, Y. *Polymer* **1988**, *29*, 2229−2234.
(55) Ringard-Lefebvre, C.; Baszkin, A. *Langmuir* **1994**, *10*, 2376−2381.
(56) Brandrup, J., Immergut, E. H., Grulke, E. A., Eds.; *Polymer Handbook*, 4th ed.; Wiley: New York, 1999.
(57) Meyerhofer, D. *J. Appl. Phys.* **1978**, *49*, 3993−3997.

MA0509006